coatings

MDPI

Article

Effect of Boron Doping Concentration on the Wettability and Surface Free Energy of Polycrystalline Boron-Doped Diamond Film

Peng Wang [1], Qiyuan Yu [1], Xiaoxi Yuan [2], Zheng Cui [1], Yaofeng Liu [1], Nan Gao [1], Huichao Jin [3,*], Shaoheng Cheng [1,*], Junsong Liu [1,*] and Hongdong Li [1]

[1] State Key Laboratory of Superhard Materials, Jilin University, Changchun 130012, China
[2] Institute for Interdisciplinary Quantum Information Technology, Jilin Engineering Normal University, Changchun 130052, China
[3] Key Laboratory of Bionic Engineering, Ministry of Education, Jilin University, Changchun 130022, China
* Correspondence: jinhc@jlu.edu.cn (H.J.); chengshaoheng@jlu.edu.cn (S.C.); jsliu@jlu.edu.cn (J.L.)

Abstract: The wettability and surface free energy of diamonds are crucial for their applications. In this study, polycrystalline boron-doped diamond (PBDD) films with different boron doping concentrations were prepared, and the effect of the boron doping concentration on the wettability and surface free energy (SFE) of the film was investigated. The SFEs of the PBDD films were investigated by employing the surface tension component approach and the equation-of-state approach. The investigation suggested that the alternative formulation of Berthelot's rule, the Lifshitz-van der Waals/acid-base (van Oss) approach, and the Owens-Wendt-Kaelble approach were suitable for estimating the SFEs of PBDD films, whereas the Fowkes approach, Berthelot's (geometric mean) combining rule, and Antonow's rule could not provide reliable results. Results showed that the SFEs of PBDD films increased with increasing boron doping concentration, and the SFEs were 43.26–49.66 mJ/m^2 (Owens-Wendt-Kaelble approach), 42.89–52.26 mJ/m^2 (Lifshitz-van der Waals/acid-base), and 44.38–48.73 mJ/m^2 (alternative formulation of Berthelot's rule). This study also provides a reference for the application of empirical and physics-based semi-empirical approaches to SFE estimation.

Keywords: diamond; surface; wettability; surface free energy

Citation: Wang, P.; Yu, Q.; Yuan, X.; Cui, Z.; Liu, Y.; Gao, N.; Jin, H.; Cheng, S.; Liu, J.; Li, H. Effect of Boron Doping Concentration on the Wettability and Surface Free Energy of Polycrystalline Boron-Doped Diamond Film. *Coatings* **2023**, *13*, 305. https://doi.org/10.3390/coatings13020305

Academic Editor: Alexander Tolstoguzov

Received: 6 January 2023
Revised: 25 January 2023
Accepted: 27 January 2023
Published: 29 January 2023

1. Introduction

As crucial parameters of surface properties, the wettability and surface free energy (SFE) of a solid can determine the diffusion behavior of molecules at the liquid–solid interface, which are important for electrochemical reactions and interface adhesion [1,2]. When coating materials are applied to different substrates, their wettability and SFE can determine their properties, including adhesion strength and anticorrosion [2]. For example, low SFE materials (e.g., Teflon and silicones) have non-sticking surfaces to resist fouling adhesion. However, their low SFEs also reduce the strength of their adhesion to substrates, thereby reducing their lifespan [3]. Diamonds, as super-hard materials, have many potential applications in various fields [4,5]. Wettability and SFE will be crucial parameters for substrate-supporting diamond films. Researchers have investigated the wettability and SFE of several types of diamonds. Zhang et al. estimated the SFEs of chemical-vapor-deposited diamonds by using a theoretical model [6]. Ma et al. studied the SFEs of H-terminated and O-terminated polycrystalline diamond films [7]. Tian et al. discussed the SFEs of the diamond films prepared in the atmosphere of CH_4/H_2, $CH_4/H_2/Ar$, and $CH_4/H_2/N_2$ [8]. Using molecular dynamics and density functional theory simulations, Skrobas et al. investigated the dependency of the SFE of nanodiamonds on particle size [9]. These studies provide an important basis for the application of diamond materials.

The contact angle (CA, θ) measurement is a simple and effective approach to determine the wettability of a solid [10,11]. The SFE of a solid (γ_{sv}) can be estimated by Young's equation [12]:

$$\gamma_{sv} = \gamma_{lv} cos\theta + \gamma_{sl} \quad (1)$$

where γ_{lv} and γ_{sl} are the SFE of the liquid-vapor and the solid–liquid interfaces, respectively. Based on Young's equation, surface tension component approaches and equation-of-state approaches have been developed to estimate SFE [13]. The former includes the Fowkes approach [14], the Owens-Wendt-Kaelble approach [15], and the Lifshitz-van der Waals/acid–base (van Oss) approach [16]. The latter includes Antonow's rule [17], Berthelot's (geometric mean) combining rule [18], and an alternative formulation of Berthelot's rule [19]. Most of these methods are empirical and semi-empirical and lack a physical basis; therefore, the applicability and accuracy of a single approach is insufficient.

Owing to the excellent inherent properties of diamonds and high electrical conductivity, polycrystalline boron-doped diamond (PBDD) films have been widely used in many fields, including those related to coating materials [20], electrochemical application [21], sensing devices for medical applications [22,23], semiconductor devices [24], micro-electro-mechanical systems (MEMS) [25], photoelectrocatalysis [26], and supercapacitors [27]. To the best of our knowledge, studies on the wettability and SFE of PBDD films are lacking. Therefore, in this study, PBDD films with different boron contents were prepared and tested. The surface chemistry and morphology of the PBDD films were studied because they can affect the wettability of solid surfaces. Because the droplet size has effects on the contact angle measurement, the effect of drop volume was also investigated. To reduce the limitations of the empirical and semi-empirical approaches, the SFEs of PBDD films were investigated using different approaches. The main purpose of this study was to find suitable approaches to estimate the SFEs of PBDD films, and to obtain reliable SFEs for use in analyzing the relationship between SFEs and boron doping concentration. We expect that the results of this study can provide a reference for the application of empirical and physics-based semi-empirical approaches.

2. Materials and Methods

2.1. Silicon Wafer Treatment

First, a silicon wafer (20220908-9A, China Electronics Science & Technology Group 46TH Institute, Tianjin, China) was abraded with diamond powder (~300 nm) to increase its roughness, which was conducive to the deposition of the diamond film. To increase the number of diamond nucleation sites, the silicon wafer was treated with an alcohol/diamond powder mixture in an ultrasonic cleaner for 60 min. Finally, the surface of the silicon wafer was cleaned with alcohol and deionized water to remove diamond powder and debris.

2.2. Deposition of PBDD Film on Silicon Wafer

PBDD films were deposited on abraded silicon wafers using micro-wave plasma chemical vapor deposition (MPCVD) at 2.45 GHz. The deposition process was performed in a mixture of hydrogen (H_2), methane (CH_4), and gaseous boron (Gas-B). Gas-B was introduced by hydrogen through a solution of trimethyl borate. PBDD films with different boron doping concentrations were prepared by adjusting the ratios of the mixture gases. The ratios of the mixture gases (H_2/CH_4/Gas-B) were 200/4/0.1 sccm (B−01), 200/4/1 sccm (B−10), 200/4/2 sccm (B−20), 200/4/3 sccm (B−30), 200/4/4 sccm (B−40), and 200/4/5 sccm (B−50). In the deposition, conditions in the reaction chamber were maintained at 8.5 KPa and 800 °C. After 11 h of deposition, the thickness of the PBDD film was approximately 7 μm.

2.3. Characterization

The surface morphologies of the PBDD films were observed via scanning electron microscopy (SEM; MAGELLAN-400, FEI Company, Hillsborough, CA, USA). The Raman spectrum was measured via Raman spectroscopy (InVia Raman microscope, Renishaw,

Gloucestershire, UK) combined with a 532-nm wavelength laser. The crystal structures of the samples were determined by X-ray diffraction (XRD; Smart Lab SE, Rigaku, Tokyo, Japan). The contact angles and surface morphology were determined by contact angle measurements (XG-CAMC33, SUNZERN, Shanghai, China) and atomic force microscopy (AFM; Cypher ES, Oxford Instrument Co., Oxford, UK), respectively. The carrier concentration was measured by the van der Pauw and Hall method (ET900g-HS, East Changing, Beijing, China).

2.4. Contact Angle Measurement

Subsequently, the PBDD films were cleaned and dried. The effect of the water drop size on the contact angle measurements was investigated. In addition, diiodomethane (Chengdu AiKe Chemical Reagent Co., Ltd., Chengdu, China) and glycerol (Shanghai Macklin Biochemical Technology Co., Ltd., Shanghai, China) were selected as additional probe liquids to investigate their contact angles on PBDD films.

3. Results and Discussion

The Raman spectrum [28] and roughness of the silicon wafer in Figure S1 show the smooth surface of the polished silicon wafer. SEM images in Figure 1a–f show that continuous PBDD films are successfully deposited on silicon wafers, and the diamonds exhibit a similar grain size, which is approximately 1–4 μm. Because a high-roughness surface can trap more air than a flat surface, the surface roughness has a significant effect on the wettability of a solid [29]. AFM measurements (Figure 1g–l) show that the root-mean-square roughness (Rq) of PBDD films is similar, ranging from 128.89 nm to 131.13 nm. Based on the SEM and AFM images in Figure 1, it can be concluded that different PBDD films have similar surface morphologies and roughness; thus, the boron doping concentration has no effect on either surface morphology or roughness.

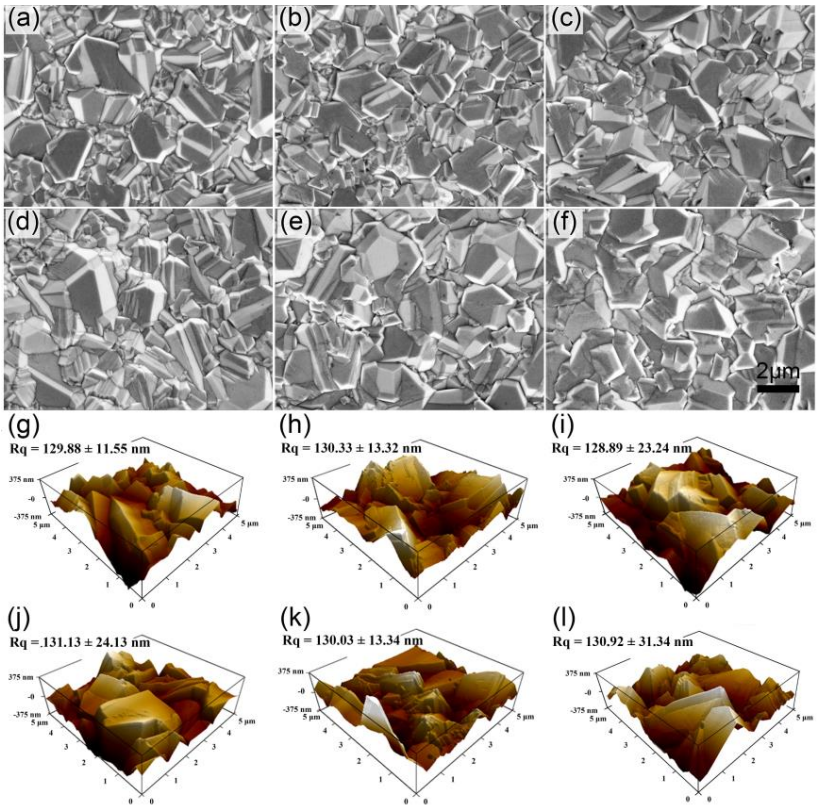

Figure 1. SEM images and the AFM measurement results of the (**a**,**g**) B−01, (**b**,**h**) B−10, (**c**,**i**) B−20, (**d**,**j**) B−30, (**e**,**k**) B−40, and (**f**,**l**) B−50 (root-mean-square roughness [Rq] is the average of three measurements for each sample).

The surface chemistry plays an important role in the wettability of solids. Hence, the surface chemistry of the PBDD films was investigated by XRD and Raman spectroscopy. Figure 2a shows the XRD patterns of the PBDD films. The peaks at 69.2° and 69.4° correspond to Si (004) and Si (100), respectively [30], and the peak at 61.7° corresponds to SiC. During the growth of the PBDD film, adamantane or carbon species firstly react with the Si surface, forming an SiC interlayer between the PBDD film and the Si substrate [31]. All PBDD films exhibit the same diamond phases with three orientations: (111), (220), and (311) [30]. The (111) peak at 43.9° exhibits the highest intensity, indicating the existence of the (111) preferred orientation. The peaks at 75.3° and 91.5° correspond to the (220) and (311) facets, respectively [32]. The three diamond peaks shift slightly to the left as the boron doping concentration increases (Figure 2a). The similar XRD patterns indicate that there are approximate relative intensities of the (111), (220), and (311) faces. Thus, all the PBDD films exhibit similar crystalline compositions.

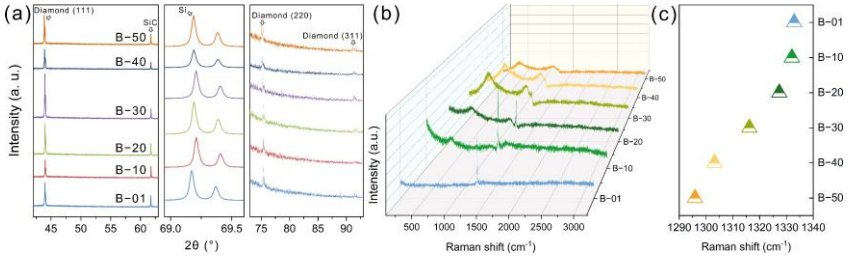

Figure 2. (**a**) XRD patterns of the PBDD films. (**b**) Raman spectra of the PBDD films. (**c**) Variation of the position of the characteristic peak of sp^3 carbon.

Raman spectroscopy was employed to investigate the changes in the boron doping concentration of the PBDD films. B−01 shows a characteristic peak of diamond at 1332 cm^{-1} (Figure 2b), and there are no broad peaks related to doped boron because of its low concentration. The Raman spectrum of the B−10 sample shows two weak peaks at 500 cm^{-1} and 1200 cm^{-1}, which correspond to the boron doping-induced Fano effect and density of states [33]. The two broad peaks gradually become distinct from those of B−10 to B−50, whereas the sp^3 peak weakens. This is because an increase in the boron doping concentration can lead to a decrease in the intensity of sp^3 peaks [34]. For both B−40 and B−50, the diamond sp^3 peaks were extremely weak to be identified, which is consistent with the characteristics of heavily boron-doped diamond [33,35]. In addition, doped boron can change the position of the sp^3 peak. Figure 2c shows a shift in the characteristic peak of sp^3 carbon to a lower wavenumber with an increase in the boron doping concentration. The downshift of this peak in the spectra of the PBDD films is caused by tensile mechanical stress [36]. Raman spectra and carrier concentration measurements (Table S1) confirmed that the boron concentration increased gradually from B−01 to B−50. B−40 and B−50 exhibited similar carrier concentrations, which may be restrained by the upper limit of the boron doping concentration. This is because the diamond films have a limited number of doping sites, and therefore, excessive doping concentrations make no difference. In this study, the boron doping concentrations of B−40 and B−50 may be close to the upper limit.

Because the probe drop size affects the contact angle measurements, DI water was first employed to clarify its effect on the PBDD film. According to the line tension effect [37], all the PBDD samples follow the same pattern of CA values changing with drop size. Therefore, to simplify the testing, the PBDD sample with an intermediate boron doping concentration, i.e., B−30, was used. The probe drop volume was set from 0.5 to 7 μL. Figure 3a shows that CAs decrease with increasing drop volume, which can be explained by the line tension effect [37], and the mean CA is 72.7°. Using the drop volume corresponding to the mean CA value has been used as a standard to measure CAs [11]. The CA of the 3.5 μL DI water is close to the mean value; thus, the 3.5 μL drop volume is a suitable choice for further measurement. Given the Lifshitz-van der Waals/acid–base (van Oss) approach is a "three-liquids" method, CAs were measured using three-probe liquid, that is, DI

water (polar solution), diiodomethane (nonpolar solution), and glycerol (polar solution). Figures 3b and S2, and Table S2 show the CA measurements of the PBDD films, which reveal that CAs decrease with increasing boron concentration.

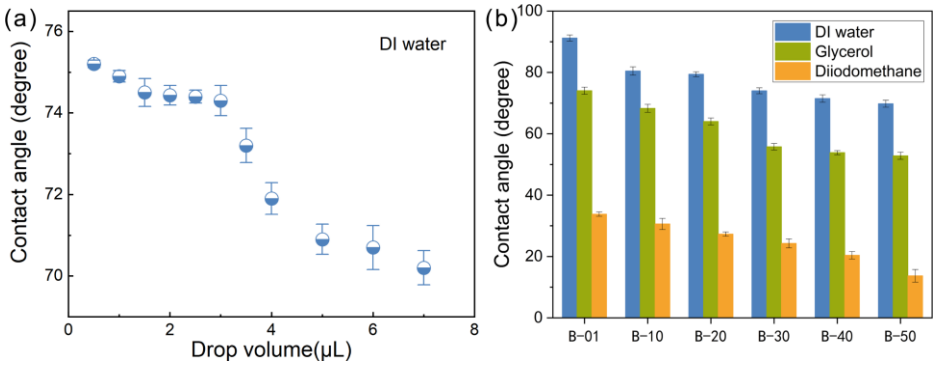

Figure 3. (**a**) Effect of drop volume on the CA measurement. (**b**) CA measurement by employing DI water, diiodomethane, and glycerol as probe liquids.

In the surface tension component approach, Fowkes proposed that the SFE of a solid is the sum of the independent surface tension components [14]:

$$\gamma_{sl} = \gamma_{sv} + \gamma_{lv} - 2\left(\gamma_{sv}^{d}\gamma_{lv}^{d}\right)^{1/2} \quad (2)$$

where γ_{sv}^{d} and γ_{lv}^{d} are the dispersive components of γ_{sv} and γ_{lv}, respectively. Combining Equations (1) and (2),

$$\gamma_{lv}cos\theta = -\gamma_{lv} + 2\left(\gamma_{sv}^{d}\gamma_{lv}^{d}\right)^{1/2} \quad (3)$$

Using the data in Figure 3b and Table S3, the SFE values of the PBDD films were estimated using Equation (3). The results in Figure 4a and Table S4 show that the SFEs increased with increasing boron doping concentration for a single-probe liquid. However, the SFEs of a single sample with different probe liquids exhibit significant differences. For a specific solid, SFE is a constant value. Hence, the Fowkes approach cannot reflect the physical facts suitable and is unsuitable for estimating the SFEs of PBDD films.

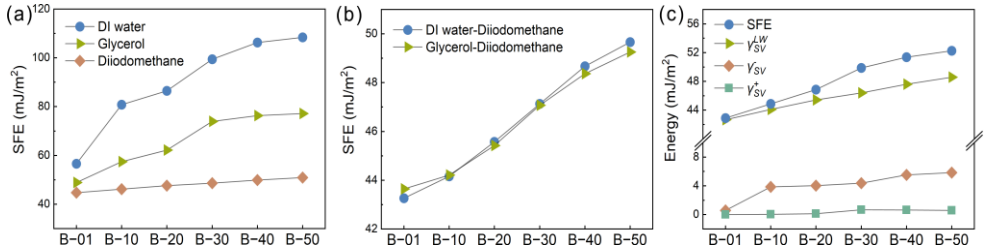

Figure 4. SFEs of the samples estimated by the (**a**) Fowkes approach and (**b**) Owens-Wendt-Kaelble approach. (**c**) SFEs, γ_{sv}^{LW}, γ_{sv}^{+}, and γ_{sv}^{-} of samples estimated by the Lifshitz-van der Waals/acid-base (van Oss) approach.

Owens and Wendt further developed a "two-liquids" approach based on the Fowkes approach, in which the solid–liquid interfacial tension (energy) fits the following equation [15]:

$$\gamma_{*v} = \gamma_{*v}^{d} + \gamma_{*v}^{p} \quad (4)$$

$$\gamma_{sl} = \gamma_{sv} + \gamma_{lv} - 2\left(\gamma_{sv}^{d}\gamma_{lv}^{d}\right)^{1/2} - 2\left(\gamma_{sv}^{p}\gamma_{lv}^{p}\right)^{1/2} \quad (5)$$

Combining Equations (1) and (5) yields:

$$\gamma_{lv}(1+cos\theta) = 2\left(\gamma_{sv}^{d}\gamma_{lv}^{d}\right)^{1/2} + 2\left(\gamma_{sv}^{p}\gamma_{lv}^{p}\right)^{1/2} \quad (6)$$

where γ_{lv}^{d} and γ_{lv}^{p} (see Table S3) represent the dispersion and polar components of the probe liquid, respectively. γ_{sv}^{d} and γ_{sv}^{p} are the dispersion and polar components of the solid, respectively. According to Equation (6), the SFEs of the PBDD films could be estimated using two-probe liquids. Two combinations (DI water-diiodomethane and glycerol-diiodomethane) were employed to estimate the SFEs of PBDD films, which provided a similar result (Figure 4b and Table S5). For a PBDD film, the SFE should be a constant value. With this in mind, the results appear to be reliable. In addition, the results show that the SFEs of the PBDD films increase with increasing boron doping concentration. B−01 exhibits the lowest SFEs of 43.26 mJ/m^2 and 43.64 mJ/m^2, and B−50 exhibits the highest SFEs of 49.66 mJ/m^2 and 49.26 mJ/m^2.

The Lifshitz-van der Waals/acid-base (van Oss) approach is an improvement over the Fowkes approach [38]. This approach uses the "three-liquids" method to estimate the SFE of a solid [16], which involves the following equations:

$$\gamma_{*v} = \gamma_{*v}^{LW} + 2\left(\gamma_{*v}^{+}\gamma_{*v}^{-}\right)^{1/2} \quad (7)$$

$$\gamma_{lv}(1+cos\theta) = 2\left(\gamma_{lv}^{LW}\gamma_{sv}^{LW}\right)^{1/2} + 2\left(\gamma_{lv}^{+}\gamma_{sv}^{-}\right)^{1/2} + 2\left(\gamma_{lv}^{-}\gamma_{sv}^{+}\right)^{1/2} \quad (8)$$

where γ_{lv}^{LW}, γ_{lv}^{+}, and γ_{lv}^{-} are the Lifshitz-van der Waals, acid, and base components of the probe liquids, respectively. γ_{sv}^{LW}, γ_{sv}^{+}, and γ_{sv}^{-} are the Lifshitz-van der Waals, acid, and base components of the solid, respectively. Based on the data in Figure 3c and Equation (8), the SEFs of the PBDD films were estimated. Figure 4c and Table S6 show that SFEs of the PBDD films range from 42.89 mJ/m^2 (B−01) to 52.26 mJ/m^2 (B−50), which are comparable to the results of the two-liquid approach. In addition, the SFEs of the PBDD films increased with increasing boron doping concentration.

The SFEs of the PBDD films obtained by the Owens-Wendt-Kaelble approach and Lifshitz-van der Waals/acid-base (van Oss) approaches are reasonable. However, several researchers have suggested that the equation-of-state approaches are closer to the fact of the experiment compared with the surface tension component approaches [13]. Hence, the SFEs of the PBDD films were also investigated using the equation-of-state approach to obtain a reliable result. Berthelot's (geometric mean) combining rule is an equation-of-state approach. The solid–liquid interfacial tension can be written as [18]

$$\gamma_{sl} = \gamma_{lv} + \gamma_{sv} - 2\sqrt{\gamma_{lv}\gamma_{sv}} = \left(\sqrt{\gamma_{lv}} - \sqrt{\gamma_{sv}}\right)^2 \quad (9)$$

Combining Equations (9) and (1),

$$cos\theta = -1 + 2\left(\frac{\gamma_{sv}}{\gamma_{lv}}\right)^{1/2} \quad (10)$$

where γ_{lv} and γ_{sv} represent the SFEs of the liquid and solid, respectively. Figure 5a and Table S7 show the SEFs estimated using Equation (10). The SFEs increased with increasing boron doping concentration, and there were large differences between the SFEs estimated using different probe liquids. Since the SFE of a specific solid should be a constant value, the results estimated using this approach are not reliable.

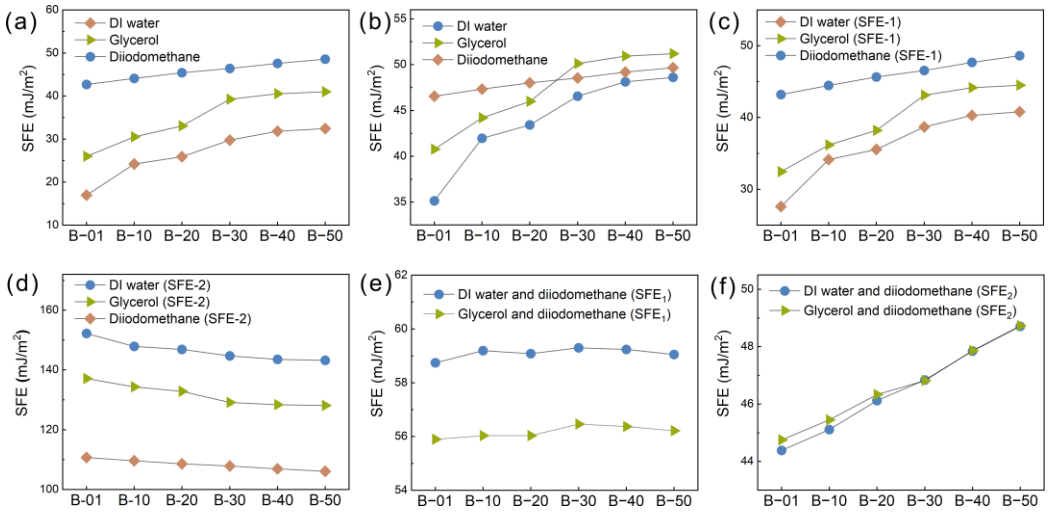

Figure 5. (**a**) SFEs of PBDD films estimated by Berthelot's rule. (**b**) SFEs of PBDD films estimated by Antonow's rule. (**c**) SFE-1 and (**d**) SFE-2 of PBDD films estimated by the alternative formulation of Berthelot's rule with $\beta = 1.057 \times 10^{-4}$ m^2/mJ. (**e**) SFE_1 and (**f**) SFE_2 estimated by the alternative formulation of Berthelot's rule with different liquid combinations.

Antonow's rule is another equation-of-state relation of the equation-of-state approaches for estimating the SFE [17]. According to Antonow's rule, the relationship between γ_{sl}, γ_{lv}, and γ_{sv} is

$$\gamma_{sl} = |\gamma_{lv} - \gamma_{sv}| \tag{11}$$

Combining Equation (11) and Young's equation yields:

$$cos\theta = -1 + 2\,\frac{\gamma_{sv}}{\gamma_{lv}} \tag{12}$$

DI water, glycerol, and diiodomethane were selected as probe solutions to estimate the PBDD film SFE. Figure 5b and Table S8 show that the SFEs estimated by different probe liquids are significantly different, which renders obtaining reliable SFEs difficult.

Given the applicable limitations of Berthelot's (geometric mean) combining rule and Antonow's rule, Kwok and Neumann proposed an alternative formulation of Berthelot's rule [19] that contains a modifying factor β:

$$cos\theta = -1 + 2\sqrt{\frac{\gamma_{sv}}{\gamma_{lv}}}\left[1 - \beta(\gamma_{lv} - \gamma_{sv})^2\right] \tag{13}$$

where β is an unknown empirical constant. Through experiments with different liquids and solids, Kwok et al. proposed that β is a constant with a value of 1.057×10^{-4} m^2/mJ. By employing the data in Figure 3c, the mentioned β value, and Equation (13), two equation solutions can be obtained—that is, SFE-1 and SFE-2 (Figure 5c,d, and Table S9). Figure 5c,d show there are large differences between the SFE values estimated using the different probe liquids. In addition, the values of SFE-2 in Figure 5d were too large to be practical and reliable; therefore, this solution is ignored. Thus, $\beta = 1.057 \times 10^{-4}$ m^2/mJ is not a suitable choice for the current SFE estimation.

Furthermore, polar–nonpolar liquid combinations, that is, DI water–diiodomethane and glycerol–diiodomethane, were used as probe liquids to estimate the SFE and β. Table S10 and Figure 5e,f show the results for SFE_1-β_1 and SFE_2-β_2. Table 1 shows that the standard deviations of both β_2 are lower than those of both β_1; hence, both β_2 can be considered reliable constant values. In addition, the SFE_1-β_1 results from different liquid combinations were significantly different (Figure 5e), whereas the SFE_2-β_2 results were comparable (Figure 5f). Based on the analysis, the results shown in Figure 5f are reliable, and the SFEs of the PBDD films are shown in Table 2.

Table 1. Modifying factor (β) estimated using Equation (13).

Combinations	Modifying Factor	Mean (m^2/mJ)	Standard Deviation (m^2/mJ)
DI water-diiodomethane	β_1	1.75×10^{-3}	±0.0003603
	β_2	3.48×10^{-4}	±0.0000656
Glycerol-diiodomethane	β_1	3.43×10^{-3}	±0.0009535
	β_2	4.36×10^{-4}	±0.0001419

Table 2. SFEs of the PBDD films.

PBDD Films	DI Water and Diiodomethane SFE_2 (m^2/mJ)	Glycerol and Diiodomethane SFE_2 (m^2/mJ)
B−01	44.38	44.75
B−10	45.11	45.45
B−20	46.12	46.33
B−30	46.84	46.82
B−40	47.85	47.86
B−50	48.71	48.73

4. Conclusions

In this study, PBDD films with different boron doping concentrations were prepared and tested. The SFEs of the PBDD films were estimated using surface tension component approaches and equation-of-state approaches. The investigation suggested that the alternative formulation of Berthelot's rule, the Lifshitz-van der Waals/acid-base (van Oss) approach, and the Owens-Wendt-Kaelble approach were suitable for estimating the SFEs of PBDD films, whereas the Fowkes approach, Berthelot's (geometric mean) combining rule, and Antonow's rule could not provide reliable results. In addition, the constant value β (1.057×10^{-4} m^2/mJ) of the alternative formulation of Berthelot's rule should be used with caution. Results showed that the SFEs of PBDD films increased with increasing boron doping concentration, and the SFEs were 43.26–49.66 mJ/m^2 (Owens-Wendt-Kaelble approach), 42.89–52.26 mJ/m^2 (Lifshitz-van der Waals/acid-base), and 44.38–48.73 mJ/m^2 (alternative formulation of Berthelot's rule). These results are similar and reliable and can provide a reference for the understanding and application of PBDD films.

Supplementary Materials: The following supporting information can be downloaded at: https://www.mdpi.com/article/10.3390/coatings13020305/s1, Figure S1: (a) Raman spectrum and (b) AFM measurement of the polished silicon wafer; Figure S2: Contact angle images of (a) B-01; (b) B-10; (c) B-20; (d) B-30; (e) B-40; and (f) B-50; Table S1: The carrier concentrations of the PBDD films with different boron doping concentration; Table S2: Contact angle measurement with DI water, diiodomethane, and glycerol; Table S3: Values of γ_{lv}, γ_{lv}^{d}, γ_{lv}^{p}, γ_{lv}^{LW}, γ_{lv}^{-}, and γ_{lv}^{+} of the probe liquids; Table S4: SFEs estimated by the Fowkes approach; Table S5: Values of γ_{sv}^{d}, γ_{sv}^{p}, and SFE estimated by the Owens-Wendt-Rabel-Kaelble approach; Table S6: Values of γ_{sv}^{LW}, γ_{sv}^{-}, γ_{sv}^{+}, and SFE estimated by the Lifshitz-van der Waals/acid-base (van Oss) approach; Table S7: SFEs estimated by the Berthelot's rule; Table S8: SFEs estimated by the Antonow's rule; Table S9: SFE-1 and SFE-2 estimated by alternative formulation of Berthelot's rule ($\beta = 1.057 \times 10^{-4}$ m^2/mJ); Table S10: β_1, SFE_1, β_2, and SFE_2 estimated by the alternative formulation of Berthelot's rule.

Author Contributions: Writing—original draft preparation, P.W.; Conceptualization, H.J., S.C., J.L. and H.L.; Investigation, Q.Y., X.Y., Z.C., Y.L. and N.G.; writing—review and editing, H.J. and H.L.; project administration, H.J., S.C., J.L. and H.L. All authors have read and agreed to the published version of the manuscript.

Funding: This work was supported by the National Natural Science Foundation of China (Grant No. 51972135) and the Key Program in Science and Technologies of Jilin Province (Grant No. 20210203167SF).

Institutional Review Board Statement: Not applicable.

Informed Consent Statement: Not applicable.

Data Availability Statement: Not applicable.

Conflicts of Interest: The authors declare no conflict of interest.

References

1. Annamalai, M.; Gopinadhan, K.; Han, S.A.; Saha, S.; Park, H.J.; Cho, E.B.; Kumar, B.; Patra, A.; Kim, S.-W.; Venkatesan, T. Surface energy and wettability of van der Waals structures. *Nanoscale* **2016**, *8*, 5764–5770. [CrossRef] [PubMed]
2. Jin, H.; Tian, L.; Bing, W.; Zhao, J.; Ren, L. Bioinspired marine antifouling coatings: Status, prospects, and future. *Prog. Mater. Sci.* **2022**, *124*, 100889.
3. Burris, D.L.; Zhao, S.; Duncan, R.; Lowitz, J.; Perry, S.S.; Schadler, L.S.; Sawyer, W.G. A route to wear resistant PTFE via trace loadings of functionalized nanofillers. *Wear* **2009**, *267*, 653–660. [CrossRef]
4. Muzyka, K.; Sun, J.; Fereja, T.H.; Lan, Y.; Zhang, W.; Xu, G. Boron-doped diamond: Current progress and challenges in view of electroanalytical applications. *Anal. Methods* **2019**, *11*, 397–414. [CrossRef]
5. Tyagi, A.; Walia, R.S.; Murtaza, Q.; Pandey, S.M.; Tyagi, P.K.; Bajaj, B. A critical review of diamond like carbon coating for wear resistance applications. *Int. J. Refract. Hard Met.* **2019**, *78*, 107–122. [CrossRef]
6. Zhang, Y.; Zhang, F.; Chen, G. Surface energies and morphologies of chemical-vapor-deposited diamond films. *J. Appl. Phys.* **1994**, *76*, 7805–7808. [CrossRef]
7. Ma, Z.-C.; Gao, N.; Cheng, S.-H.; Liu, J.-S.; Yang, M.-C.; Wang, P.; Feng, Z.-Y.; Wang, Q.-L.; Li, H.-D. Wettability and Surface Energy of Hydrogen- and Oxygen-Terminated Diamond Films. *Chin. Phys. Lett.* **2020**, *37*, 046801. [CrossRef]
8. Tian, S.; Xu, F.; Sun, S.; Zhao, Y.C.; Wang, X.; Zuo, D.W. Growth rate and surface free energy of diamond films using different gas-sources. *Surf. Eng.* **2020**, *36*, 379–385. [CrossRef]
9. Skrobas, K.; Stefanska-Skrobas, K.; Stelmakh, S.; Gierlotka, S.; Palosz, B. Surface free energy of diamond nanocrystals—A molecular dynamics study of its size dependence. *Phys. Chem. Chem. Phys.* **2021**, *23*, 11075–11081. [CrossRef]
10. Zhao, T.; Jiang, L. Contact angle measurement of natural materials. *Colloids Surf. B* **2018**, *161*, 324–330. [CrossRef]
11. Han, B.; Wang, P.; Jin, H.; Hou, Z.; Bai, X. Wettability and surface energy of parylene F deposited on PDMS. *Phys. Lett. A* **2020**, *384*, 126628. [CrossRef]
12. Young, T., III. An essay on the cohesion of fluids. *Philos. Trans. R. Soc. Lond.* **1805**, *95*, 65–87.
13. Kwok, D.Y.; Neumann, A.W. Contact angle measurement and contact angle interpretation. *Adv. Colloid Interface Sci.* **1999**, *81*, 167–249. [CrossRef]
14. Fowkes, F.M. Attractive forces at interfaces. *Ind. Eng. Chem. Res.* **1964**, *56*, 40–52. [CrossRef]
15. Owens, D.K.; Wendt, R.C. Estimation of the surface free energy of polymers. *J. Appl. Polym. Sci.* **1969**, *13*, 1741–1747. [CrossRef]
16. Van Oss, C.J.; Chaudhury, M.K.; Good, R.J. Interfacial Lifshitz-van der Waals and polar interactions in macroscopic systems. *Chem. Rev.* **1988**, *88*, 927–941. [CrossRef]
17. Antonow, G.N. Sur la tension superficielle à la limite de deux couches. *J. Chim. Phys.* **1907**, *5*, 372–385. [CrossRef]
18. Daniel, B. Sur le mélange des gaz. *Compt. Rendus* **1898**, *126*, 1703–1706.
19. Kwok, D.Y.; Neumann, A.W. Contact angle interpretation in terms of solid surface tension. *Colloids Surf. A Physicochem. Eng. Asp.* **2000**, *161*, 31–48. [CrossRef]
20. Sharma, D.K.; Girão, A.V.; Chapon, P.; Neto, M.A.; Oliveira, F.J.; Silva, R.F. Advances in RF glow discharge optical emission spectrometry characterization of intrinsic and boron-doped diamond coatings. *ACS Appl. Mater. Interfaces* **2022**, *14*, 7405–7416. [CrossRef]
21. de Oliveira Silva, K.N.; Rodrigo, M.A.; dos Santos, E.V. Electrochemical treatment of soil-washing effluent with boron-doped diamond electrodes: A review. *Curr. Opin. Solid State Mater. Sci.* **2021**, *25*, 100962. [CrossRef]
22. Lan, Y.; Coetsier, C.; Causserand, C.; Groenen Serrano, K. An experimental and modelling study of the electrochemical oxidation of pharmaceuticals using a boron-doped diamond anode. *Chem. Eng. J.* **2018**, *333*, 486–494. [CrossRef]
23. Li, H.; Zhou, K.; Cao, J.; Wei, Q.; Lin, C.-T.; Pei, S.E.; Ma, L.; Hu, N.; Guo, Y.; Deng, Z.; et al. A novel modification to boron-doped diamond electrode for enhanced, selective detection of dopamine in human serum. *Carbon* **2021**, *171*, 16–28. [CrossRef]
24. Choi, U.; Kwak, T.; Han, S.; Kim, S.-W.; Nam, O. High breakdown voltage of boron-doped diamond metal semiconductor field effect transistor grown on freestanding heteroepitaxial diamond substrate. *Diam. Relat. Mater.* **2022**, *121*, 108782. [CrossRef]
25. Zhu, X.; Aslam, D.M. CVD diamond thin film technology for MEMS packaging. *Diam. Relat. Mater.* **2006**, *15*, 254–258. [CrossRef]
26. Guo, C.; Zheng, J.; Deng, H.; Shi, P.; Zhao, G. Photoelectrocatalytic interface of boron-doped diamond: Modification, functionalization and environmental applications. *Carbon* **2021**, *175*, 454–466. [CrossRef]
27. Wang, J.; He, Z.; Tan, X.; Wang, T.; Liu, L.; He, X.; Liu, X.D.; Zhang, L.; Du, K. High-performance 2.6 V aqueous symmetric supercapacitor based on porous boron-doped diamond via regrowth of diamond nanoparticles. *Carbon* **2020**, *160*, 71–79. [CrossRef]
28. Hu, C.-X.; Xiao, Q.; Ren, Y.-Y.; Zhao, M.; Dun, G.-H.; Wu, H.-R.; Li, X.-Y.; Yang, Q.-Q.; Sun, B.; Peng, Y.; et al. Polymer Ionic Liquid Stabilized Black Phosphorus for Environmental Robust Flexible Optoelectronics. *Adv. Funct. Mater.* **2018**, *28*, 1805311. [CrossRef]
29. Hideo, N.; Ryuichi, I.; Yosuke, H.; Hiroyuki, S. Effects of surface roughness on wettability. *Acta Mater.* **1998**, *46*, 2313–2318. [CrossRef]

30. Yao, K.; Dai, B.; Tan, X.; Yang, L.; Zhao, J.; Ralchenko, V.; Shu, G.; Liu, K.; Han, J.; Zhu, J. Microwave plasma-assisted chemical vapor deposition of microcrystalline diamond films via graphite etching under different hydrogen flow rates. *CrystEngComm* **2019**, *21*, 2502–2507. [CrossRef]
31. Tiwari, R.N.; Chang, L. Growth, microstructure, and field-emission properties of synthesized diamond film on adamantane-coated silicon substrate by microwave plasma chemical vapor deposition. *J. Appl. Phys.* **2010**, *107*, 103305. [CrossRef]
32. Zhang, Z.; Lin, C.; Yang, X.; Tian, Y.; Gao, C.; Li, K.; Zang, J.; Yang, X.; Dong, L.; Shan, C. Solar-blind imaging based on 2-inch polycrystalline diamond photodetector linear array. *Carbon* **2021**, *173*, 427–432. [CrossRef]
33. Mortet, V.; Živcová, Z.V.; Taylor, A.; Davydová, M.; Frank, O.; Hubík, P.; Lorincik, J.; Aleshin, M. Determination of atomic boron concentration in heavily boron-doped diamond by Raman spectroscopy. *Diam. Relat. Mater.* **2019**, *93*, 54–58. [CrossRef]
34. Ndao, A.N.; Zenia, F.; Deneuville, A.; Bernard, M.; Lévy-Clément, C. Effect of boron concentration on the electrochemical reduction of nitrates on polycrystalline diamond electrodes. *Diam. Relat. Mater.* **2000**, *9*, 1175–1180. [CrossRef]
35. Lévy-Clément, C.; Ndao, N.A.; Katty, A.; Bernard, M.; Deneuville, A.; Comninellis, C.; Fujishima, A. Boron doped diamond electrodes for nitrate elimination in concentrated wastewater. *Diam. Relat. Mater.* **2003**, *12*, 606–612. [CrossRef]
36. Girolami, M.; Bellucci, A.; Mastellone, M.; Orlando, S.; Serpente, V.; Valentini, V.; Polini, R.; Sani, E.; De Caro, T.; Trucchi, D.M. femtosecond-laser nanostructuring of black diamond films under different gas environments. *Materials* **2020**, *13*, 5761. [CrossRef]
37. Gu, Y. Drop size dependence of contact angles of oil drops on a solid surface in water. *Colloids Surf. A Physicochem. Eng. Asp.* **2001**, *181*, 215–224. [CrossRef]
38. Ho, C.C.; Khew, M.C. Surface free energy analysis of natural and modified natural rubber latex films by contact angle method. *Langmuir* **2000**, *16*, 1407–1414. [CrossRef]